Published in final edited form as:

Nano Lett. 2015 December 9; 15(12): 8032–8043. doi:10.1021/acs.nanolett.5b03370.

Multifunctional MRI/PET Nanobeacons Derived from the in Situ Self-Assembly of Translational Polymers and Clinical Cargo through Coalescent Intermolecular Forces

Charalambos Kaittanis[†,‡], **Travis M. Shaffer**[†,§], **Alexander Bolaender**[†], **Zachary Appelbaum**[†], **Jeremy Appelbaum**[†], **Gabriela Chiosis**[†], and **Jan Grimm**[*,†,||,⊥,#]

[†]Molecular Pharmacology Program, Memorial Sloan Kettering Cancer Center, 1275 York Avenue, New York, New York 10065, United States

[||]Department of Radiology, Memorial Sloan Kettering Cancer Center, 1275 York Avenue, New York, New York 10065, United States

[‡]Center for Advanced Medical Imaging Sciences, Department of Radiology, Massachusetts General Hospital, 55 Fruit Street, Boston, Massachusetts 02114, United States

[§]Department of Chemistry, Hunter College and Graduate Center of the City University of New York, New York, New York 10065, United States

[⊥]Department of Pharmacology, Weill Cornell Medical College, New York, New York 10065, United States

[#]Department of Radiology, Weill Cornell Medical College, New York, New York 10065, United States

Abstract

[*]Corresponding Author: grimmj@mskcc.org.

Present Address

(C.K.) Center for Advanced Medical Imaging Sciences, Department of Radiology, Massachusetts General Hospital, 55 Fruit Street, Boston, Massachusetts 02114, United States.

ASSOCIATED CONTENT

Supporting Information

The Supporting Information is available free of charge on the ACS Publications website at DOI: 10.1021/acs.nanolett. 5b03370. Physical characterization of polymeric nanophores loaded with gadolinium, ^{89}Zr-PNP stability, AFM of (un)loaded PNP, cytotoxicity profile of Doxo-PNP and in vivo studies with clodrosomes. (PDF)

Notes

The authors declare no competing financial interest.

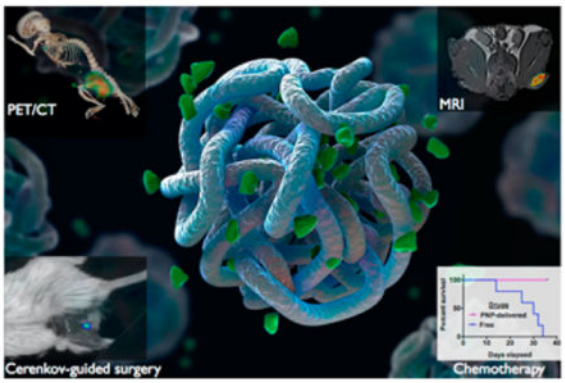

Novel multifunctional platforms are needed for oncology in order to assist physicians during surgery and chemotherapy. In the present study, we show that polymeric nanobeacons, consisting of the glucose-based polymer dextran, can be used to guide surgery and improve drug delivery. For imaging, the nanobeacons stably retained the positron emitter 89-zirconium and the MRI contrast agent gadolinium, without the need of a chelator. In addition to using them for PET imaging, the ^{89}Zr-nanobeacons guided the surgical resection of sentinel lymph nodes, utilizing their inherent Cerenkov luminescence. Through weak electrostatic interactions, the nanoparticles carried combinations of chemotherapeutics for the simultaneous inhibition of oncogenic pathways, resulting in enhanced tumor regression. The nanobeacons also allowed monitoring of drug release via MRI, through the quenching of the gadolinium signal by the coloaded drug, making them a new multifunctional theranostic nanotechnology platform for the clinic.

Keywords

Lymph node resection; Cerenkov-guided surgery; combination therapy

Effective cancer treatment relies on successful surgical resection of the primary tumor and possibly tumor-draining lymph nodes, as well as delivery of therapeutic drugs at the site of the disease, in order to lower the tumor burden and prevent recurrence and metastasts.[1–3] Specifically, the drug (or combinations thereof) has to reach the tumor at adequate concentrations to accomplish tumor regression, prevent emergence of drug resistant cell populations, and avert development of a metastatic niche. Therefore, it is desirable that therapeutic compounds stay in circulation for sufficient time in order to reach the tumor without affecting healthy organs.[4,5] Nanotechnology has addressed this urgent clinical need with the introduction of novel drug delivery platforms, including liposomes and polymeric nanoparticles that are either in the clinic or ongoing clinical trials.[6–8] For example, the liposomal formulation Doxil (Doxorubicin) and AmBisome (Amphotericin B) offer enhanced pharmacokinetics and high drug delivery of compounds with poor aqueous solubility.[9,10] The drug release mechanism of these vehicles relies on either plasma membrane fusion or the enzymatic activity of lipases, which may cause side effects and hepatic toxicity. In the case of polymeric nanoparticles that are constructed with polymers such as poly(lactic-*co*-glycolic) acid (PLGA) and hydrophobiccore polyesters (HBPE), the therapeutic cargo is released when the polymer undergoes acid hydrolysis, usually in the late

endosomal and lysosomal compartments, or in the presence of lytic enzymes, like esterases.[11–14] More recently, other potentially translational nanostructures, including nanoparticles made of melanin, have been created, in order to address important clinical needs.[15,16]

Recently, we reported that the clinical formulation of polymer-coated iron oxide nanoparticles (Ferumoxytol, Feraheme) could serve as drug delivery system in cancer chemotherapy.[17] Specifically, the dextran coating of the nanoparticles retained diverse therapeutic payloads via weak electrostatic interactions. Once perturbed, such as by mild acidification of their microenvironment or local elevation of the ionic strength, the particles rapidly released their cargo. This microenvironment-driven mechanism was utilized for the treatment of solid cancers, taking advantage of the tumor's aberrant metabolism and enhanced glycolytic activity that lowers stromal and interstitial pH. In addition to improved therapy, the spatiotemporal drug release was monitored via MRI because release of the cargo restored Ferumoxytol's spin– spin (T2) and spin–lattice (T1) relaxation signals while leaving the T2* signature unaltered. Such a self-reporting multifunctional drug delivery platform is a promising translational vehicle because neither the particle nor the drug is subject to any chemical modification, which could lead to a faster administrative approval process. However, a theoretical drawback of the use of Ferumoxytol for drug delivery or imaging might be iron overloading of patients, such as for certain drugs that may require repeated administrations over a long period or large dosages of Ferumoxytol to provide adequate MR contrast.[18,19] Therefore, we hypothesized that dextran-based nanophores of comparable size could serve as facile drug delivery carrier, amenable to rapid transition from the lab to the patient bedside, averting the risk of iron overloading with Feraheme-based drug delivery. We also reasoned that our polymeric nanophores (PNPs) could accommodate radio-tracers without the use of chelating molecules, making them suitable as facile imaging constructs for oncologic interventions. Herein, we report that clinically utilized high-molecular-weight dextran, applied as plasma substitution and rheological improvement with few rare side effects to a very small fraction of patients, can indeed retain therapeutics at physiological conditions and differentially release them upon acidification of the local microenvironment. These PNPs showed improved efficacy in vitro and in vivo when compared to free drugs, and they accomplished enhanced tumor regression through the simultaneous inhibition of oncogenic pathways in breast and prostate cancer models.

Because surgery remains the principal therapeutic intervention in oncology for many cancers, complete removal of the malignant tissue and affected lymph nodes is required in an effort to minimize recurrence and distal metastasis.[20,21] To accomplish this, oncologists rely on medical information derived through preoperative imaging modalities, such as positron emission tomography (PET) and the use of radiotracers, including fluorodeoxyglucose (^{18}F-FDG) and the ^{99m}Tc-radiocolloid.[22,23] The current clinical standard agent to image sentinel lymph nodes is the sulfur colloid nanoparticle, which is labeled with ^{99m}Tc that allows preoperative imaging via planar lymphoscintigraphy or single-photon emission computed tomography (SPECT) and intraoperative guidance with a hand-held gamma probe. Novel multimodal agents consisting of materials already used in the clinic can serve as diagnostic platforms and decision-support tools before and during surgery in order to facilitate better therapeutic course-of-action with improved outcome with

surgeons not deviating from their standard workflow. Recent examples have shown how optical and spectroscopic approaches can support decision-making in oncologic surgery.[24–29] From fluorescent molecular probes to multimodal nanoparticles, researchers provided the first tools to assist surgeons in the removal of primary tumors and tumor-draining lymph nodes. Toward this goal, herein we show that nanobeacons constructed from a clinically approved polymer (dextran) that has benign characteristics and little toxicity can provide superior diagnostic capabilities, combining the high sensitivity and resolution of positron emission tomography (PET) and the intraoperative imaging capability of Cerenkov luminescence for the optically guided resection of lymph nodes. In addition to surgery, the PNP can serve as a drug delivery vehicle with an activatable MRI signal to report drug release, making them a translational nanoplatform for integrated, personalized cancer therapy.

Results and Discussion

Considering that dextran polymers lack any intrinsic clinical imaging capabilities, we investigated first whether dextran could form nanobeacons via the chelator-free retention of metals, such as gadolinium (Gd) for magnetic resonance imaging (MRI) and radiometals for PET. We opted to first examine whether dextran can chelate Gd to also provide a nonradioactive imaging agent. The dextran PNP sequestered Gd from a Gd salt (gadolinium acetate) solution after heating for 30 min at 70 °C and firmly retained it after filtration, which subsequently decreased the nanophore's T1 magnetic resonance signal (Figure 1A). Because increase in the solution's ionic strength impaired chelation (Figure 1B), the PNP chelation mechanism likely relies on the electrostatic associations between the nanophore and the metal ion, which is similar to the previous observation on dextran-coated Feraheme[17] but differs from the recently reported oxophilicity- based chelation with silica nanoparticles.[30] We next determined the long-term serum and pH stability of Gd-chelating PNPs that were either loaded at high or room temperature. Chelation of Gd by PNPs at 70 °C achieved PNPs that could retain gadolinium for a week in serum (Figure 1C) and withhold it even at pH 6.0 (Figure 1D). However, PNPs that chelated Gd at room temperature gradually released gadolinium in serum with complete unloading occurring after 4 days (Supporting Information Figure S1A). Furthermore, these PNPs released gadolinium at pH 6.0 with approximately half of the gadolinium found outside the PNPs after 2 h Supporting Information Figure S1B). Although the heating-based chelation approach with PNPs increased the nanoparticles size (from an average diameter of 34 nm at 25 °C to a diameter of 82 nm after heating at 70 °C for the unloaded PNPs) as determined via dynamic light scattering, the PNPs had diameters below 100 nm and their surface charge remained unaltered (Figure 1E,F), indicating that this strategy may provide reasonably stable imaging agents and also allow tuning of the retention characteristics as needed. It is possible that heating caused cross-linking and entanglement of dextran molecules, causing larger PNP formation and tighter Gd retention, explaining the difference in serum stability between chelation at 25 and 70 °C. We furthermore examined whether the molecular weight of the dextran that the PNPs are made of plays a role in the retention of gadolinium. Our results indicated that PNPs composed of high-molecular-weight dextran were able to retain more Gd than their counterparts consisting of lower molecular weight dextran, likely due to the

presence of more chelating domains in the large polymers (Supporting Information Figure S1C,D), making PNPs of high-molecular-weight dextran a more attractive carrier of molecular cargo.

Intriguingly, similar to Gd the PNPs sequestered also the positron emitting radiometal ^{89}Zr (Figure 2A), which has a half-life of 78.4 h, ideal for the tracking of long-circulating entities and allowing for PET imaging. Considering that at room temperature the PNPs partially bound ^{89}Zr (49.2% binding, $diameter_{PNP}$ = 34 nm) as indicated by the presence of the free zirconium peak in the radio ITLC chromatogram, we attempted chelating zirconium with PNPs under heating conditions (30 min, 70 °C), where the PNPs achieved complete binding to the radionuclide (100% binding, $diameter_{PNP}$ = 82 nm; Supporting Information Figure S2A). The resulting radiolabeled PNPs securely held their radioactive cargo in water and serum, as well as under EDTA-challenging conditions (Supporting Information Figure S2B). Specifically, the EDTA challenge test assesses the strength of the interaction between a radionuclide and a chelator, so if the ^{89}Zr-PNP association were weak EDTA would have stripped off ^{89}Zr from the PNPs. Because multimodality with a common imaging agent is frequently desired through the oncologic clinical workflow, we sought to utilize the light generated during the decay of radionuclides, such as ^{89}Zr, that occurs due to the charged positron's super- relativistic speed (Cerenkov luminescence, CL).[31,32] The ^{89}Zr-retaining PNPs exhibited Cerenkov luminescence in vitro and in vivo (Figure 2B and E,F), which hints at their potential use as intraoperative imaging agents, for example, for localization of sentinel lymph nodes, providing important decision-making information using optical systems and cameras to collect the Cerenkov light. In a proof of concept study based on the current practice of lymph node biopsy collection that requires local administration of the Isosulafan Blue dye and/or ^{99m}Tc Sulfa-colloid, we injected ^{89}Zr-PNPs that were prepared through our heat-assisted procedure intracutaneously in the paw of mice or peritumorally around xenografts located on the animals' flanks. Through PET/CT imaging, we observed drainage of the PNPs to local and higher echelon lymph nodes (Figure 2C and Supporting Information Figure S2C), which are the primary sites of early metastasis due to their proximity to the tumor and sites readily infiltrated by tumor-associated macrophages[33] and thus requiring removal. Biodistribution studies confirmed PNP retention in the lymph nodes with ultimate clearance through the hepatobiliary route (Figure 2D), indicating a transition into a systemic phase out of the lymphatic system 24 h after administration. This allowed for ^{89}Zr-PNP-guided surgical removal of sentinel lymph nodes using Cerenkov luminescence signal (Figure 2E,F). Apart from lymph node resection based on PNP's luminescence, a surgeon may accomplish this task through PNP's multimodality once the radiolabeled nanoparticles carry fluorophores that can be excited by the broad-spectrum Cerenkov light, as previously demonstrated by our group.[30] This might be of major importance for highly aggressive tumors, such as triple-negative breast cancer and castration-resistant prostate cancer, where the surgeon has to eliminate disease burden, by removing the lesion and lymph nodes, to prevent recurrence and metastasis, as subsequent therapeutic options are limited. As current lymph node resection methods are visual and have limited sensitivity, oncologists may either miss some affected lymph nodes, which can serve as sites of distal metastasis, or remove healthy lymph nodes. Therefore, these findings

may translate to the use of PNPs for sensitive lymph node detection in the clinic, using a facile chelation strategy with an already FDA-approved nanoplatform.

Since translational drug vehicles are urgently needed in oncology, we examined whether the PNP nanoplatform can be utilized for the delivery of chemotherapeutics in solid tumors. Working toward this direction and bearing in mind that many advanced chemotherapeutics have poor aqueous solubility, we prepared solutions with different concentrations of the fluorophore DiI as an easily quantifiable, prototypic hydrophobic high-molecular-weight cargo in a mixed solvent system. Under continuous gentle stirring, a fixed concentration of PNP was added dropwise into the mixed-solvent (water/DMSO) solution of DiI. After purification to remove any unbound fluorophore, we determined the nanoparticles' retention (scavenging) efficiency spectrophotometrically by comparing the absorbance/fluorescence emission of the nanoparticle-scavenged and original solutions (Figure 3A). Interestingly, when comparing equal concentrations of dextran PNPs and Ferumoxytol (dextran-coated iron oxide nanoparticles, utilized previously in ref 17), the dextran nanoparticles even more effectively sequestered DiI than Ferumoxytol (Figure 3A). This is attributed to dextran's thicker polymer layer and the ability of cargo to more extensively associate with it via weak electrostatic interactions. On the other hand, although PNPs and Ferumoxytol have similar size, some functional groups involved in cargo retention might be utilized for the association of the dextran with the iron oxide core, rendering Ferumoxytol a less efficient cargo carrier. The cargo retention was more efficient close to neutral pH but it was impaired in acidic conditions (Figure 3B), showing the importance of functional group availability for PNP loading. Because dextran's molecular weight dictated the degree of gadolinium retention, we studied whether this parameter similarly affected the sequestration of larger molecular payload, such as DiI (MW: 933.88). PNP preparations formulated with different dextrans were tested with the PNPs made of high-molecular-weight dextran having the highest scavenging efficiency (76.4 ± 3.2%, Figure 3C), likely due to the bigger polymer's more functional groups and microcavities that might be involved in cargo sequestration. This may provide versatility during chemotherapy, where low-and high-molecular-weight PNP may be used for drug delivery, improving therapy outcome, and lowering treatment side effects.

Next we tested whether cargo retention and encapsulation, as well as release, affect the structure of the PNPs. Because the scavenging of DiI by PNPs did not affect their size (Figure 3D), after loading the PNPs via the solvent diffusion method and purifying them through dialysis we determined their size with DLS. Loading of cargo neither affected the size (Figure 3E) nor the surface charge (Figure 3F) of the PNPs, likely due to retention of the molecular payload within the PNPs' internal cavities that provide hydrophobic sites and an extensive network of weak electrostatic associations, such as hydrogen bonds and van der Waals forces, leaving the polymer's surface groups to interact with water molecules consisting of the nanoparticle solvation sphere. The long-term serum stability of the cargo-loaded PNPs was first determined using nanophores loaded with the hydrophobic near-infrared fluorophore DiR. During the course of a week, no changes in the PNPs' fluorescence were detected, demonstrating that the nanophores can stably retain their cargo at physiological conditions (Figure 3G). However, release of the cargo, including chemotherapeutics such as doxorubicin, was triggered by micro-environmental alterations, like the acidification of the aquatic milieu. For instance, the doxorubicin-carrying PNPs

rapidly released the drug once the pH dropped below 7.0, such as pH 6.8 that is encountered in many solid tumors (Figure 3H). Atomic force microscopy confirmed that the PNPs preserved their size after microenvironment-driven cargo release (Supporting Information Figure S3A–C), further supporting the notion that the cargo loading and release processes do not affect PNPs' physical characteristics, hence its pharmacokinetics properties remain unaltered. Doxorubicin was released in a slightly faster rate at pH 6.0 than pH 6.8, possibly due to the wider perturbation of the electrostatic forces holding the drug within the nanoparticle at this pH level, making PNP an environmental-responsive drug delivery platform.

Subsequently, we next investigated the dextran PNPs' therapeutic potential in vitro. Cell viability studies using the human prostatic adenocarcinoma cell line PC3 showed that doxorubicin-loaded PNP had a lower IC50 than free drug (3.1 vs 6.5 μM, Supporting Information Figure S4). Because combination therapy is often employed in cancer treatment in order to suppress different molecular pathways and address disease heterogeneity, we loaded PNPs with a combination of drugs. Specifically for the treatment of castration-resistant prostate cancer, we coloaded PNPs with enzalutamide (MDV- 3100, Xtandi) and the PI3K inhibitor BEZ235 (diameter_{PNP} = 34 nm; drug-loading efficiency 64 ± 5%). This drug combination was selected because it was previously reported that inhibition of the androgen receptor pathway leads to overactivation of the PI3K cascade, while suppression of PI3K upregulates androgen-receptor-mediated signaling (Figure 4A).[34] Studies with the androgen-responsive human prostate cancer cell line LNCaP showed that PNP-based drug delivery was more effective that administration of the drugs in their free form (Figure 4A). Apart from prostate cancer, we investigated whether the nanophores could be used for combinatorial therapy of other tumors, such as triple-negative breast cancer, where it was recently shown that treatment with doxorubicin and an EGFR inhibitor led to enhanced cell death and tumor regression.[35] We coloaded doxorubicin and the MEK inhibitor AZD6244 (Selumetinib) into dextran nanophores, since MEK is a downstream target of EGFR (diameter_{PNP} = 34 nm; drugloading efficiency 78 ± 8%). Treatment of the human breast cancer cells MDA-MB-468 with the doxorubicin/AZD6244- loaded PNPs achieved higher cell death at lower dosages than the free drug combination (Figure 4B). Although chemotherapy with drug-loaded Ferumoxytol did not cause any toxicity from the iron oxide core to mice undergoing acute chemotherapy,[17] a potential translational limitation of the use of Ferumoxytol as a drug delivery vehicle for repeated chemotherapy administrations in the clinic is the possibility of iron overloading. Hence, we examined whether dextran-based nanophores could be used for the treatment of solid tumors in vivo. We first determined the biodistribution of drug-loaded PNPs (room-temperature loading, diameter_{PNP} = 34 nm), using nanophores that were loaded with the ^{131}I-radiolabeled Hsp90 inhibitor PU-H71 because the radiolabeling method involves substitution of the drug's "cold" iodine (^{127}I) with ^{131}I, thus preserving the drug's structure. Following iv administration of either free or PNP-loaded PU-H71, the animals were euthanized after 4 and 24 h, and the radioactivity of the collected organs was measured on a gamma counter, showing increased drug levels in the tumors of animals that received the PNP-based chemotherapy (Figure 4C–E, Supporting Information Figure S4B–D). It should be noted that retention of PU-H71 by the intracellular machinery depends on the presence of Hsp90 complexes, when the chaperone associates

with oncogenic client proteins.[36] Otherwise in the absence of high-affinity Hsp90-client complexes, the drug is exported outside the cell and eventually excreted by the body through the kidneys and liver. Collectively these results show that drug delivery with PNPs improves the drug's homing at the tumor and uptake by cells, making this chemotherapeutic vehicle an attractive approach for the treatment of tumors.

In an effort to address tumor heterogeneity and improve therapy for prevalent cancers, in vivo combinatorial chemotherapy and simultaneous delivery of drugs to concurrently inhibit major oncogenic pathways and cellular processes was performed in prostate and breast cancer models (room-temperature loading, $diameter_{PNP}$ = 34 nm). Studies with athymic male nude mice bearing xenografts of the androgen-receptor- positive human prostatic adenocarcinoma cell line LNCaP showed that dextran nanophores coloaded with MDV3100 and BEZ235 (B/M-PNP) were able to achieve tumor regression, as opposed to the free drugs that had much less of an effect (Figure 5A,B). Long-term treatment of mice bearing human triple-negative breast cancer xenografts (MDA-MB-468) with the nanophores demonstrated improved survival and tumor regression (Figure 5C,D), contrary to the same dose of free drugs. To exclude the possibility that the nanophores' therapeutic effect was due to uptake by and subsequent death of tumor-associated macrophages, we treated LNCaP tumor-bearing animals with liposome-encapsulated clodronate (Clodrosomes) that targets macrophages and causes their depletion. Considering the findings that treatment with clodrosomes did not cause any tumor growth suppression and regression in these tumors (Supporting Information Figure S5), the drugloaded nanophores primarily exert their therapeutic activity directly on the tumor through improved delivery and microenvironment-based release of their cargo and not due to toxic effects on macrophages.

Finally, we examined whether PNPs can serve as a translational multifunctional platform, allowing the noninvasive monitoring of drug delivery. Because the PNPs retained gadolinium and various chemotherapeutics, we reasoned that the presence of drug molecules around the gadolinium ion might affect the magnetic properties of Gd-loaded nanoparticles. In order to test this hypothesis, we first chelated Gd with PNPs under heating ($diameter_{PNP}$ = 82 nm). Subsequently, we loaded these PNPs that had high or low levels of gadolinium with different amounts of the fluorophore DiI at room temperature and then imaged these formulations using MRI. Intriguingly, the spin–spin (T1) and spin–lattice (T2) relaxation signal of the PNP solution was high at high DiI concentrations, whereas at lower dye levels the T1 and T2 parameters were closer to those of the PNPs that carried only Gd (Figure 6A,B). This was also observed when we loaded two drugs (Doxorubicin and Flutax1) into the same PNP (Supporting Information Figure S6). However, the T2* signal was not affected by the dye's presence (Figure 6C), which prompted us to investigate whether the dye, as a molecular payload, affects the diffusion of water molecules from the vicinity of the Gd atom, reminiscent of what we previously observed in drug-loaded Ferumoxytol, where the cargo hindered the diffusion of water molecules within the nanoparticle. Utilizing MRI to measure the PNP preparations' apparent diffusion coefficient (ADC), we determined that once loaded with drugs the ADC of PNPs decreased, negatively correlating to the levels of the nanophores' cargo (Figure 6D,E). These findings prompted us to examine whether Gd/doxorubicin-loaded PNPs could be used for the simultaneous monitoring of drug release and nanoparticle homing in vivo with the same translational vehicle. We accomplished this by

monitoring the T1 and T2* signal via MRI, where after 4 h after iv administration, the tumor T1 signal of mice receiving the Gd/doxorubicin-loaded PNPs was higher than that of animals injected with control Gd-loaded PNP, yet no apparent differences in the tumor T2* signal between these cohorts (Figure 7A–D). Twenty-four hours after treatment, the T1 and T2* of the two experimental groups were similar, showing that doxorubicin was successfully released in vivo and demonstrating that PNPs can be used as a theranostic nanosystem in oncology.

Conclusion

Overall, we demonstrated that polymeric dextran-based nanophores could be used for combinatorial therapy and chelation of medically relevant tracers. Because retention of the payload is mediated via weak electrostatic interactions that do not physically or chemically alter the cargo or the nanoparticles, we envision that these nanophores could serve as translational chemotherapeutic carriers without receiving extensive scrutiny from regulatory agencies. With the emergence of new therapeutic interventions and novel imaging platforms for the operating room, as well as with the present finding that the gadolinium signal can be quenched by another molecular cargo, PNPs may improve clinical decision-making and patient care, by providing vital information, such as sentinel lymph node drainage and metastasis, and improving the outcome of chemotherapy. Particularly for single or combination drug therapy in the treatment of solid tumors, the PNP provide an elegant platform that allows the physician to obtain accurate spatiotemporal information on the drug's distribution and accumulation in the body noninvasively, allowing fine-tuning of the treatment regiment tailored to the patient's characteristics. From the perspective of drug development and pharmaceutical R&D, the PNP may assist in the design of better clinical trials by providing key pharmacokinetic information, based on quantitative clinical imaging and use of the cargo-facilitated quenching of the MR signal, without subjecting the drugs to a chemical modification or using radioactivity. The translation of these polymeric nanophores to areas other than oncology, such as infectious disease and inflammatory syndromes, is anticipated, opening new nanoscale- based therapeutic venues. Overall, the PNP may improve survival, lower side effects and provide better patient life quality at the dawn of precision medicine, using today's building blocks and tools mantled together through nanotechnology's new knowledge.

Materials and Methods

Chemicals

Dextran (MW: 10 000, 100 000 and 450 000–650 000), gadolinium acetate, and DMSO were obtained from Sigma-Aldrich (St Louis, MO). The fluorophores DiI and DiR were purchased from Life Technologies (Carlsbad, CA), Flutax1 from Tocris Bioscience (Minneapolis, MN), whereas Doxorubicin, AZD6244, BEZ235, and MDV3100 from Selleck Chemicals (Houston, TX). The clodrosomes (liposomal clodronate) were bought from Encapsula NanoSciences, LLC (Brentwood, TN).

PNP Characterization

The size of the nanoparticles was determined through dynamic light scattering (Nano-ZS, Malvern, Westborough, MA), and the same instrument was used to measure the PNPs' surface charge (ζ potential). Atomic force microscopy was performed at the MSKCC Molecular Cytology Core Facility, using an Asylym Research MFP-3D-BIO instrument in tapping mode after depositing the PNPs onto AP-mica.

Animal Models

The animals were obtained from Harlan Laboratories, and all animal studies were done in accordance with protocols approved by the Institutional Animal Care and Use Committee of Memorial Sloan Kettering Cancer Center, following the National Institutes of Health guidelines for animal welfare.

Loading of PNPs with Gadolinium

High-molecular-weight dextran (10 mg) was dissolved in 200 μL of a mixed solvent system (85:15 distilled water/DMSO) and sonicated for 20 min at room temperature. The resulting solution was added dropwise to 300 μL of the gadolinium-containing solution, under stirring conditions, followed by dialysis in a microvolume chamber (MWCO: 3000, Fisher Scientific, Waltham, MA) against 1× PBS and under gentle stirring for 8 h. For loading of the dextran under heating conditions, the dextran solution was added stepwise in 25 μL intervals to the gadolinium solution under mixing at 70 °C using an Eppendorf thermomixer, followed by a 30 min mixing at this temperature. Determination of the amount of gadolinium retained by the PNPs was achieved by comparing the T1 signal of the PNP preparation with respect to known concentration of gadolinium dissolved in 1X PBS, based on T1 readings on a 0.47T mq20 NMR analyzer (Minispec, Bruker, Billerica, MA). The T1 sequence varied the interpulse spacing from 5 ms up to 8,500 ms. Similarly, assessment of the PNP loading efficiency at different salt concentrations was performed after addition of the carbohydrate solution in NaCl-containing solutions of gadolinium, which was followed by dialysis in 1X PBS and relaxometer-based measurements. To assess the loading efficiency of PNP consisting of either 10, 100, or 450–650 kDa dextran, the PNPs were incubated with the same concentration of gadolinium ([Gd] = 50 nM) at 70 °C for 30 min, followed by dialysis and characterization as described above. In order to determine the serum stability of the gadolinium-carrying PNPs, experiments were performed at 37 °C in 100% fetal bovine serum (FBS, Gemini Bio-Products, West Sacramento, CA; total volume = 200 μL). Samples were analyzed as described for gadolinium retention efficiency. Stability at different pH was determined by placing the PNPs in a dialysis chamber and incubating them in various pH conditions, while measuring tthe PNP solution's T1 signal with the Minispec relaxometer.

Radiolabeling of PNPs with ^{89}Zr

Zirconium-89 ($t_{1/2}$ = 78.4 h) was either purchased from 3D Imaging, LLC (Maumelle, AR) or produced at Memorial Sloan Kettering Cancer Center on a TR19/9 cyclotron (Ebco Industries Inc., Richmond, BC, Canada) via the ^{89}Y(p,n)^{89}Zr reaction and purified as previously described.[37] 1.0 M sodium carbonate was used to bring the ^{89}Zr-oxalate solution

to neutral pH. The neutralized ^{89}Zr solution (100 μCi) was then added to the PNP solutions, brought to 70 °C at 500 rpm on an Eppendorf thermomixer, and incubated for 1 h. To determine the radiochemical yield (% of radioactivity bound to the PNPs, 1 μL samples were taken from samples for instant thin-layer chromatography (ITLC) analysis, using silica-gel-impregnated ITLC paper (Agilent Technologies, Santa Clara, CA). The mobile phase was 50 mM EDTA (pH 5.5) with analysis on a Bioscan AR-2000 radio- TLC plate reader. Unbound ^{89}Zr travels with the mobile front, while bound ^{89}Zr is immobilized at the origin. Radiochemical yield was determined by drawing regions of interest over the origin (bound ^{89}Zr) and comparing this to the total signal. Serum stability experiments were performed at 37 °C in 50% fetal bovine serum (FBS, Gemini Bioproducts), 50% H_2O (total volume = 150 μL) or 50% mouse serum (EMD Millipore), 50% H_2O (total volume = 150 μL). Samples were analyzed as described for radiochemical yield.

PET/CT Imaging Peritumoral Model

Male nude athymic mice (8–10 weeks old, n = 3) were injected with 1 million DU145 cells in matrigel and tumors were allowed to grow for 3 weeks. Peritumoral, subcutaneous injections were done with 95–105 μCi (3.515–3.885 MBq) of ^{89}Zr-radiolabeled PNP (10 mg dextran) in 100 μL 1X PBS buffer. At 24 h, animals were anesthetized with isoflurane (Baxter Healthcare, Deerfield, IL) and oxygen gas mixture (2% for induction, 1% for maintenance) and PET/CT scans were performed using an Inveon PET/CT scanner (Siemens, Washington, DC.. Whole body PET static scans were performed, recording a minimum of 40 million coincident events with scan durations of 10–20 min. The energy and coincidence timing windows were 350–750 keV and 6 ns, respectively. The image data were normalized to correct for nonuniformity of response of the PET, dead-time count losses, positron branching ratio, and physical decay to the time of injection, but no attenuation, scatter, or partial-volume averaging correction was applied. The images were analyzed using the Inveon Research software (Siemens).

PET/CT Lymph Node Studies

For ^{89}Zr-PNP lymph node imaging studies, three mice were injected subcutaneously in the footpad with 25–35 μCi (0.925–1.295 MBq) of ^{89}Zr-PNP in 20–30 μL 1X PBS. All mice were induced with 2.5% isoflurane and maintained on 2–2.5% isoflurane in preparation for the scans. Whole body scans were performed using Inveon Multimodality (MM) CT scanner (Siemens) and Inveon dedicated PET scanner for a total of 15–45 min, and images were analyzed as described for PET/CT peritumoral imaging. Cerenkov-based surgical resection of draining lymph nodes was performed after imaging the euthanized animals on an Ivis Spectrum scanner (PerkinElmer, Waltham, MA).

CT Imaging

Whole body standard low-magnification CT scans were performed with the X-ray tube setup at a voltage of 80 kV and current of 500 μA. The CT scan was acquired using 120 rotational steps for a total of 220° yielding an estimated scan time of 120 s with an exposure time of 145 ms per frame.

Loading of Molecular Cargo into PNPs

The hydrophobic cargo (dyes and chemotherapy drugs) were dissolved in DMSO and then diluted in a mixed solvent solution, consisting of water and DMSO (50:50 v/v; total volume = 400 μL). To this solution, the dextran solution (10 mg/100 μL) was added dropwise under vortexing (1 000 rpm) at room temperature. Subsequently, the preparations were subjected to dialysis in a dialysis chamber (MWCO 3000, Fisher Scientific) against 1X PBS, followed by storage in the dark at 4 °C. Loading of Ferumoxytol (Feraheme, AMAG Pharmaceuticals, Lexington, MA) was performed as previously reported. Determination of the nanoparticles' loading was achieved spectrophotometrically using a SpectraMax M5 instrument (Molecular Devices, Sunnyvale, CA) and through HPLC after subjecting the PNPs to enzymatic degradation by Dextranase (Sigma- Aldrich). To determine the loading efficiency of PNP, made of either 10, 100, or 450–650 kDa dextran, the DiI solution ([DiI] = 5 nM) was added dropwise to the dextran solution under vortexing. The resulting PNP suspensions were dialyzed and then the amount of dye retained was determined spectrophotometrically (DiI: λ_{ex} = 549 nm, λ_{em} = 565 nM). Changes in the T2 magnetic signal of PNP attributed to cargo retention were measured on the Minispec analyzer, using a CPMG pulse-echo train with a 1.5 ms interpulse spacing. Serum and pH stability of the loaded PNPs were performed as mentioned before for the gadolinium-PNPs with fluorescence emission of the PNP preparation being assessed on the SpectraMax M5 plate reader and presence of free cargo outside the dialysis chamber with a Beckman Coulter HPLC instrument equipped with a C18 reverse phase column or fluorimetry ($\varepsilon_{Doxorubicin}$ = 11 500 M^{-1} cm^{-1} at 480 nm, ε_{DiR} = 270 000 M^{-1} cm^{-1} at 748 nm). To examine whether the presence of cargo affected the magnetic properties of gadolinium-loaded PNP (dextran 450–650 kDa, chelation at 70 °C and purified as described above) the nanoparticles were loaded with DiI using the solvent-diffusion method, followed by dialysis. Phantoms of the nanoparticle preparations were spotted on a custom-made sample holder, which was imaged on a 4.7 T animal MRI (Bruker Biospin, Billerica, MA), equipped with a 35 mm radiofrequency coil.

Serum Stability of ^{131}I-PU-H71

Radio-HPLC was performed on a Shimadzu HPLC system equipped with 2LC -10AT pumps and an SPD-M10AVP photodiode array detector (Columbia, MD), and a Lablogic Scan-RAM Radio-TLC/HPLC detector (Brandon, FL). Analytic runs were performed on a C18 Waters Atlantis T3 column (6 × 250 mm, 5 mm). The solvent system included water (solvent A) and acetonitrile (MeCN) (solvent B) for the purification and quality control of the radiotracers with a gradient of 5–95% B between 0 and 15 min and 100% B between 15 and 25 min. For serum stability, ^{131}I-PU-H71 was incubated with agitation (550 rpm) at 37 °C in 500 μL of mouse serum. At each prescribed time-point, 100 μL of the solution was removed and placed into a 1.7 mL centrifuge tube and 100 μL of cold acetonitrile was added to the serum; the resultant mixture was vortexed and centrifuged at 14 000 rpm for 5 min. After this, the clear supernatant was removed, moved to a new 1.7 mL centrifuge tube, and centrifuged again at 14 000 rpm for 5 min. The clear supernatant from this second spin was then injected into the HPLC. The residual protein from the centrifuge spins was checked for radioactivity, and only minimal residual activity remained (<1% of the starting ^{131}I). The fraction of intact ^{131}I-PU- H71 was determined by integrating the peak corresponding to the

compound and dividing by the integral over the whole HPLC run [0:100 MeCN/H_2O (both with 0.1% TFA) to 100:0 MeCN/H_2O over 25 min, t_R = 11.7 min].

Cell Viability and in Vivo Studies

PC3, LNCaP, and MDA-MB- 468 cells were obtained from ATCC (Manassas, VA) and maintained according to the supplier's instructions. To evaluate the drug-loaded PNPs toxicity profile PC3, LNCaP, and MDAMB- 468 cells were seeded on black-walled, clear bottom 96- well plates at a cell density of 10 000 cells per well, supplemented with 100 μL of 10% FBS-containing RPMI medium. Controls included cells incubated with unloaded nanoparticles or DMSO, corresponding to the free drug's final solvent concentration. Dose–response curves were obtained after the cells were treated for 48 h with corresponding agent. Subsequently, the old medium was aspirated, and cell viability was assessed via the Alamar Blue method (Life Technologies, Carlsbad, CA). The cells were supplemented with 10% Alamar blue-containing medium (10% FBS-containing RPMI), followed by 3 h incubation in a humidified incubator (37 °C, 5% CO_2) and fluorescence emission was recorded (λ_{exc} = 565 nm, λ_{em} = 585 nm) with the SpectraMax M5 plate reader. Biodistribution studies were conducted by administering iv either free or PNP-retained ^{131}I-PU-H71 to adult, male, nude mice that had PC3 xenografts on their flanks. At 4 and 24 h, the mice were euthanized, and the radioactivity of the organs was measured with a PerkinElmer Wizard^2 2480 Automatic Gamma Counter (Waltham, MA). The difference in drug uptake conferred by the PNP was determined by the equation ($Uptake_{PNP\text{-}drug} - Uptake_{free\text{-}drug}$)/$Uptake_{free\text{-}drug}$. Adult, male, nude mice (n = 9) that had bilateral LNCaP tumors on their flanks were treated iv on days 0, 2, 4, and 6 with 100 μL of equimolar ([BEZ235] = 250 μM, [MDV3100] = 100 μM) concentrations of either free (diluted in 5% DMSO-containing 1X PBS) or dual-drug-loaded PNPs. Control animals were treated with 5% DMSO-containing 1X PBS, and tumor volume was measured with calipers. For the triple-negative breast cancer model, adult, female, nude mice (n = 12) that had bilateral MDA-MB-468 xenografts on their flanks were administered iv every other day for 40 days 100 μL of equimolar ([Doxorubicin] = 500 μM, [AZD6244] = 100 μM) concentrations of either free (diluted in 5% DMSO-containing 1X PBS) or dual-drug-loaded PNPs. Treatment with clodrosomes was performed according to the supplier's protocol, whereas toxicity profile of drug-loaded Ferumoxytol was conducted at the MSKCC Comparative Pathology Lab, using nude male mice that had PC3 xenografts and were treated daily for 14 days with 100 μL iv administration of equimolar concentrations of ([Doxorubicin] = 500 μM) free or Ferumoxytol-loaded Doxorubicin. Control animals received either 100 μL of 5% DMSO-containing 1X PBS or Ferumoxytol that had the same iron concentration as the drug-loaded nanoparticle ([Fe] = 0.75 mg/mL). In vivo drug release was assessed after iv administration of equimolar Gd doses ([Gd] = 50 nM) of gadolinium-loaded PNP or gadolinium/doxorubicincoloaded PNP to adult, male, nude mice that had PC3 xenografts on their flanks. The mice were imaged with the 4.7 T Bruker Biospin MRI and a 35 mm radiofrequency coil.

Supplementary Material

Refer to Web version on PubMed Central for supplementary material.

Acknowledgments

This study was supported by the Prostate Cancer Foundation (to C.K.), Alex's Lemonade Stand Foundation (to C.K.), and Starr Cancer Consortium (I4-A427 to J.G.). This research was also partially supported by Mr. William H. and Mrs. Alice Goodwin, the Commonwealth Foundation for Cancer Research, the Center for Experimental Therapeutics of Memorial Sloan Kettering Cancer Center, the Center of Molecular Imaging and Nanotechnology and the NIH funds 1R01CA183953-01A1 and R01EB014944 (all to J.G.). T.M.S. is funded by a National Science Foundation Integrative Graduate Education and Research Traineeship (DGS 0965983 at Hunter College). This study was supported by the Department of Defense Prostate Cancer Research Program of the Congressionally Directed Medical Research Programs under Award No. W81XWH-12-1-0509 to J.G. (opinions, interpretations, conclusions and recommendations are those of the author and are not necessarily endorsed by the funding agency). The authors thank the staff of the MSKCC animal MRI core for providing expert technical assistance. Technical services provided by the MSKCC Small Animal Imaging Core Facility were supported in part by the MSKCC NIH Core Grant (P30-CA008748) and NIH Shared Instrumentation Grant 1 S10 OD016207-01, which provided funding support for the purchase of the Inveon PET/CT. Funding for the AMF was provided by a Core Support Grant of MSKCC's Experimental Therapeutics Center (to J.G. as Co-PI).

References

1. Alitalo A, Detmar M. Oncogene. 2012; 31(42):4499–4508. [PubMed: 22179834]
2. Alitalo K, Tammela T, Petrova TV. Nature. 2005; 438(7070):946–953. [PubMed: 16355212]
3. Benson JR, Jatoi I. Future Oncol. 2014; 10(4):577–586. [PubMed: 24754590]
4. Blanco E, Hsiao A, Ruiz-Esparza GU, Landry MG, Meric-Bernstam F, Ferrari M. Mol Oncol. 2011; 5(6):492–503. [PubMed: 22071376]
5. Schroeder A, Heller DA, Winslow MM, Dahlman JE, Pratt GW, Langer R, Jacks T, Anderson DG. Nat Rev Cancer. 2011; 12(1):39–50. [PubMed: 22193407]
6. Kaittanis C, Shaffer TM, Thorek DL, Grimm J. Crit Rev Oncog. 2014; 19(3–4):143–176. [PubMed: 25271430]
7. Kiessling F, Mertens ME, Grimm J, Lammers T. Radiology. 2014; 273(1):10–28. [PubMed: 25247562]
8. Prakash S, Malhotra M, Shao W, Tomaro-Duchesneau C, Abbasi S. Adv Drug Delivery Rev. 2011; 63(14–15):1340–1351.
9. O'Brien ME, Wigler N, Inbar M, Rosso R, Grischke E, Santoro A, Catane R, Kieback DG, Tomczak P, Ackland SP, Orlandi F, Mellars L, Alland L, Tendler C, Group CBCS. Ann Oncol. 2004; 15(3):440–449. [PubMed: 14998846]
10. Ringden O, Meunier F, Tollemar J, Ricci P, Tura S, Kuse E, Viviani MA, Gorin NC, Klastersky J, Fenaux P, et al. J Antimicrob Chemother. 1991; 28(Suppl B):73–82. [PubMed: 1778894]
11. Hrkach J, Von Hoff D, Ali MM, Andrianova E, Auer J, Campbell T, De Witt D, Figa M, Figueiredo M, Horhota A, Low S, McDonnell K, Peeke E, Retnarajan B, Sabnis A, Schnipper E, Song JJ, Song YH, Summa J, Tompsett D, Troiano G, Van Geen Hoven T, Wright J, LoRusso P, Kantoff PW, Bander NH, Sweeney C, Farokhzad OC, Langer R, Zale S. Sci Transl Med. 2012; 4(128):128ra39.
12. McCarthy JR, Perez JM, Bruckner C, Weissleder R. Nano Lett. 2005; 5(12):2552–2556. [PubMed: 16351214]
13. Santra S, Kaittanis C, Perez JM. Mol Pharmaceutics. 2010; 7(4):1209–1222.
14. Santra S, Kaittanis C, Perez JM. Langmuir. 2010; 26(8):5364–5373. [PubMed: 19957939]
15. Fan Q, Cheng K, Hu X, Ma X, Zhang R, Yang M, Lu X, Xing L, Huang W, Gambhir SS, Cheng Z. J Am Chem Soc. 2014; 136(43):15185–15194. [PubMed: 25292385]
16. Zhang R, Fan Q, Yang M, Cheng K, Lu X, Zhang L, Huang W, Cheng Z. Adv Mater. 2015; 27(34):5063–5069. [PubMed: 26222210]
17. Kaittanis C, Shaffer TM, Ogirala A, Santra S, Perez JM, Chiosis G, Li Y, Josephson L, Grimm J. Nat Commun. 2014; 5:3384. [PubMed: 24594970]
18. Iv M, Telischak N, Feng D, Holdsworth SJ, Yeom KW, Daldrup-Link HE. Nanomedicine (London, U K). 2015; 10(6):993–1018.

19. Khurana A, Chapelin F, Beck G, Lenkov OD, Donig J, Nejadnik H, Messing S, Derugin N, Chan RC, Gaur A, Sennino B, McDonald DM, Kempen PJ, Tikhomirov GA, Rao J, Daldrup-Link HE. Radiology. 2013; 269(1):186–197. [PubMed: 23850832]
20. Cousins A, Thompson SK, Wedding AB, Thierry B. Biotechnol Adv. 2014; 32(2):269–279. [PubMed: 24189095]
21. Wilhelm AJ, Mijnhout GS, Franssen EJ. Eur J Nucl Med. 1999; 26:S36–S42. [PubMed: 10199931]
22. Thorek DL, Abou DS, Beattie BJ, Bartlett RM, Huang R, Zanzonico PB, Grimm J. J Nucl Med. 2012; 53(9):1438–1445. [PubMed: 22872741]
23. Ravizzini G, Turkbey B, Barrett T, Kobayashi H, Choyke PL. Wiley Interdiscip Rev: Nanomed Nanobiotechnol. 2009; 1(6):610–623. [PubMed: 20049820]
24. Kircher MF, de la Zerda A, Jokerst JV, Zavaleta CL, Kempen PJ, Mittra E, Pitter K, Huang R, Campos C, Habte F, Sinclair R, Brennan CW, Mellinghoff IK, Holland EC, Gambhir SS. Nat Med. 2012; 18(5):829–834. [PubMed: 22504484]
25. Kobayashi H, Hama Y, Koyama Y, Barrett T, Regino CA, Urano Y, Choyke PL. Nano Lett. 2007; 7(6):1711–1716. [PubMed: 17530812]
26. Polom W, Markuszewski M, Rho YS, Matuszewski M. Cent Eur J Urol. 2014; 67(2):142–148.
27. Thorek DL, Ulmert D, Diop NF, Lupu ME, Doran MG, Huang R, Abou DS, Larson SM, Grimm J. Nat Commun. 2014; 5:3097. [PubMed: 24445347]
28. van Dam GM, Themelis G, Crane LM, Harlaar NJ, Pleijhuis RG, Kelder W, Sarantopoulos A, de Jong JS, Arts HJ, van der Zee AG, Bart J, Low PS, Ntziachristos V. Nat Med. 2011; 17(10):1315–1319. [PubMed: 21926976]
29. Rabin O, Manuel Perez J, Grimm J, Wojtkiewicz G, Weissleder R. Nat Mater. 2006; 5(2):118–122. [PubMed: 16444262]
30. Shaffer TM, Wall MA, Harmsen S, Longo VA, Drain CM, Kircher MF, Grimm J. Nano Lett. 2015; 15(2):864–868. [PubMed: 25559467]
31. Das S, Thorek DL, Grimm J. AdvCancer Res. 2014; 124:213–234.
32. Thorek DL, Ogirala A, Beattie BJ, Grimm J. Nat Med. 2013; 19(10):1345–1350. [PubMed: 24013701]
33. Kurahara H, Takao S, Maemura K, Mataki Y, Kuwahata T, Maeda K, Sakoda M, Iino S, Ishigami S, Ueno S, Shinchi H, Natsugoe S. Pancreas. 2013; 42(1):155–159. [PubMed: 22699204]
34. Carver BS, Chapinski C, Wongvipat J, Hieronymus H, Chen Y, Chandarlapaty S, Arora VK, Le C, Koutcher J, Scher H, Scardino PT, Rosen N, Sawyers CL. Cancer Cell. 2011; 19(5):575–586. [PubMed: 21575859]
35. Lee MJ, Ye AS, Gardino AK, Heijink AM, Sorger PK, MacBeath G, Yaffe MB. Cell. 2012; 149(4):780–794. [PubMed: 22579283]
36. Moulick K, Ahn JH, Zong H, Rodina A, Cerchietti L, Gomes DaGama EM, Caldas-Lopes E, Beebe K, Perna F, Hatzi K, Vu LP, Zhao X, Zatorska D, Taldone T, Smith-Jones P, Alpaugh M, Gross SS, Pillarsetty N, Ku T, Lewis JS, Larson SM, Levine R, Erdjument-Bromage H, Guzman ML, Nimer SD, Melnick A, Neckers L, Chiosis G. Nat Chem Biol. 2011; 7(11):818–826. [PubMed: 21946277]
37. Holland JP, Sheh Y, Lewis JS. Nucl Med Biol. 2009; 36(7):729–739. [PubMed: 19720285]

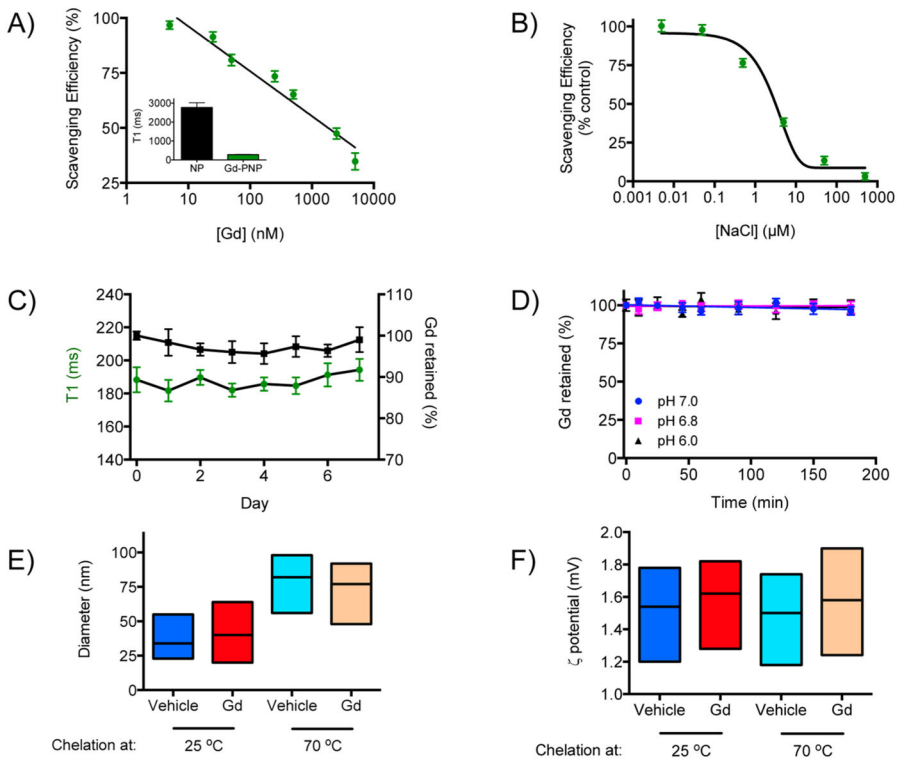

Figure 1.

Retention of the magnetic resonance tracer gadolinium with PNPs. (A) The T1 contrast agent Gd was scavenged by the polysaccharidebased PNPs at room temperature, which was associated with a marked change in the PNPs' T1 signal (inset, [Gd] = 50 nM). (B) High salt concentration impaired the PNPs' ability to sequester Gd, suggesting that the PNP–Gd association was based on weak electrostatic interactions. (C) The Gd-loaded PNPs were stable in serum during the course of a week, and (D) they withheld their cargo at different pH. (E) Heating of the PNPs increased their size but (F) did not affect their surface charge. Means ± SEM.

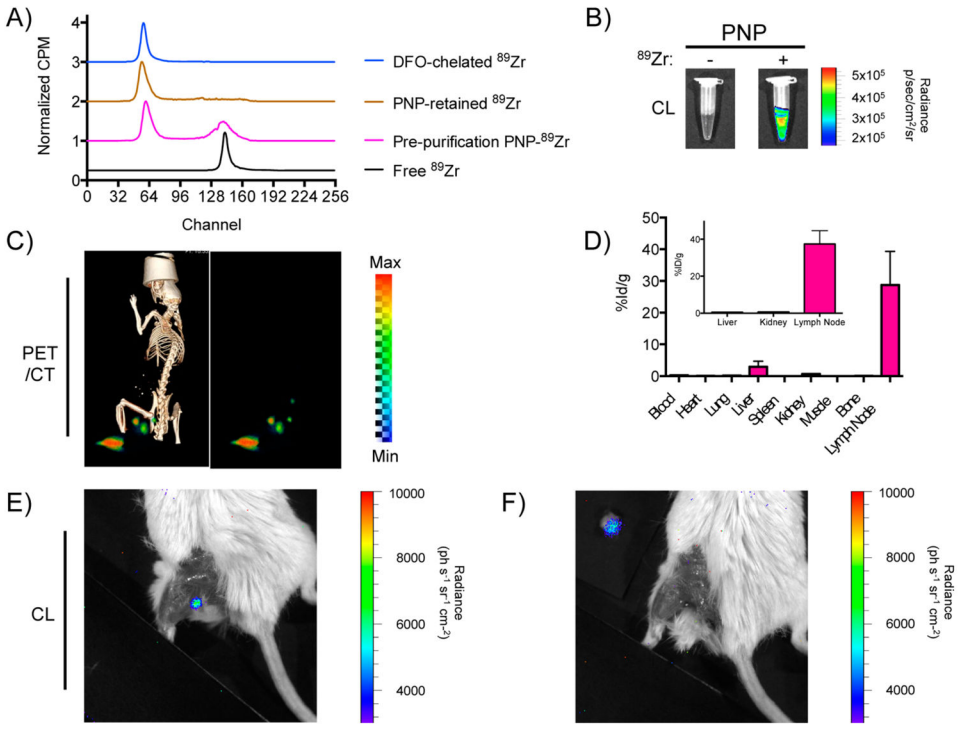

Figure 2.

PNPs for chelator-free ^{89}Zr radiolabeling. (A) PNPs chelated the PET tracer ^{89}Zr at room temperature with good efficacy when compared to the chelator desferrioxamine (DFO), according to radiochemical instant thin layer chromatograms. (B) The ^{89}Zr-retaining PNPs exhibited Cerenkov luminescence. (C) PET-CT (left) and PET only (right) lymph node imaging 24 h after injection of intrinsically labeled ^{89}Zr-PNPs in the left paw. The popliteal, superficial inguinal, and iliac lymph nodes are seen. (D) Biodistribution of ^{89}Zr-PNPs 1 h post injection in the paw (inset, 24 h after); n = 3 per time point; means ± SEM. (E,F) Surgical resection of a draining popliteal lymph node using ^{89}Zr-PNPs and Cerenkovluminescence 24 h post injection in the paw. The injection side is covered to prevent saturation. In (E), the resected node exhibiting Cerenkov luminescence is seen positioned adjacent to the animal with no signal remaining in the surgical bed.

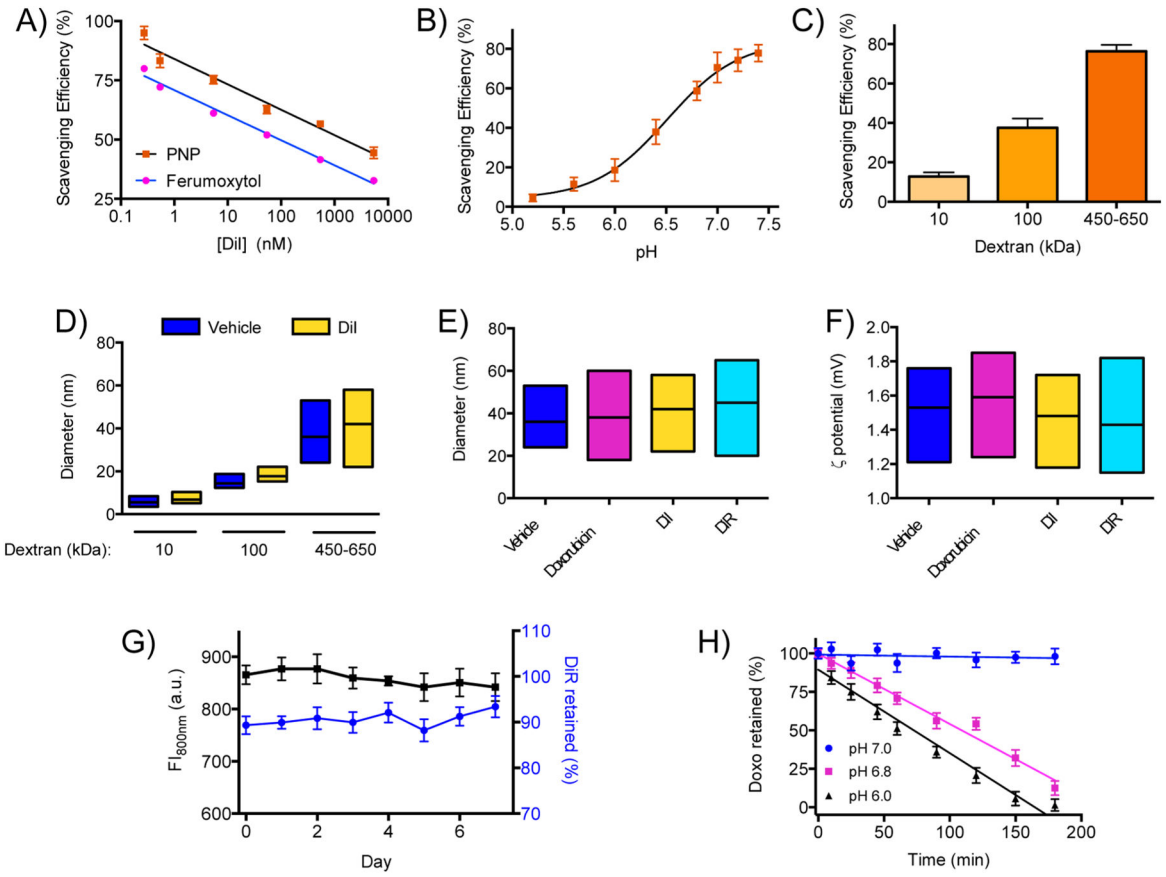

Figure 3.

Retention of molecular cargo with PNPs. (A) The dextran PNPs were able to sequester more molecules of the hydrophobic fluorophore DiI from a mixed-solvent solution than dextran-coated nanoparticles that have an iron oxide core (Ferumoxytol). (B) The PNPs sequestered less cargo (DiI) in acidic conditions. (C) PNP of high-molecular-weight dextran scavenged more DiI, which was used as a model molecular cargo. (D) The retention of DiI by the PNPs did not affect their size and nanoparticle distribution. (E) PNPs loaded with different molecules had similar size distribution to unloaded nanoparticles (vehicle), and (F) their surface charge was unaltered. (G) Serum stability of DiR-loaded PNPs, indicating long-term retention of the cargo by the polymeric nanoparticles. (H) Acidification of the microenvironment led to rapid release of the cargo from the PNPs (Doxo = doxorubicin). Means ± SEM.

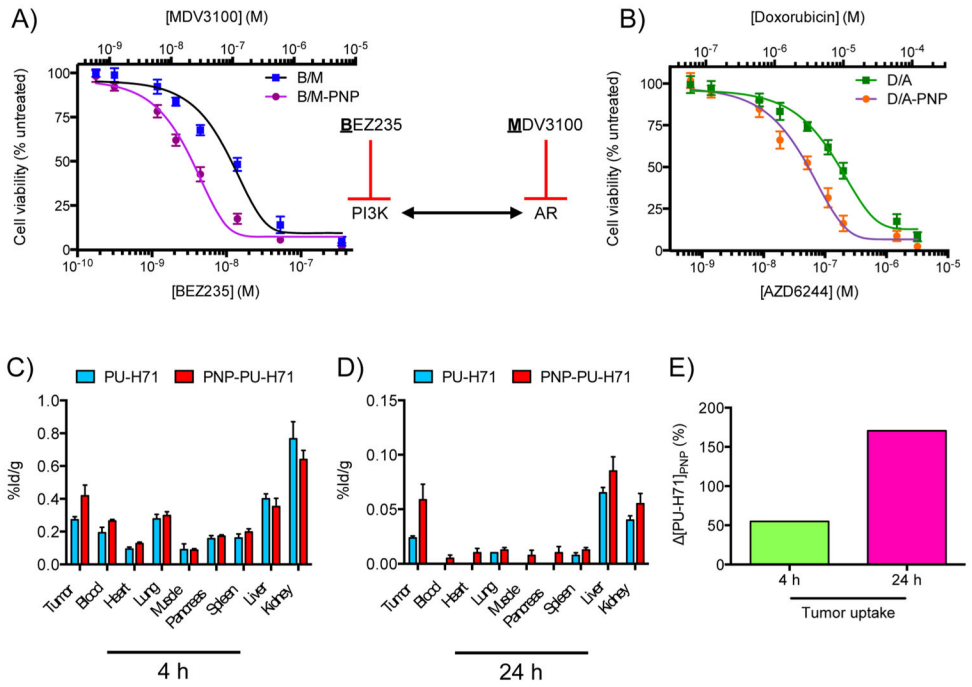

Figure 4.

Delivery with PNP improves drug efficacy in vitro and tumor uptake. (A) Simultaneous inhibition of the PI3K pathway with BEZ235 and the androgen receptor (AR) cascade with MDV3100, which were loaded on the same PNP, led to higher cytotoxicity toward the AR-positive human prostate cancer cells (LNCaP) than the drugs administered in their free forms. (B) PNP-based concurrent delivery of doxorubicin and AZD6244 was more effective than the free drugs in vitro (human breast cancer cells MDA-MB-468). (C,D) Biodistribution profiles of the free and PNP-delivered ^{131}I-PU-H71 4 and 24 h after iv administration (%ID/g: % injected dose/tissue mass; $n_{free\_4h} = 3$, $n_{PNP\_4h} = n_{free\_24h} = n_{PNP\_24h} = 4$). (E) Net change in drug delivery and retention achieved with the PNPs ($\Delta[PU\text{-}H71]_{PNP}$). Means ± SEM.

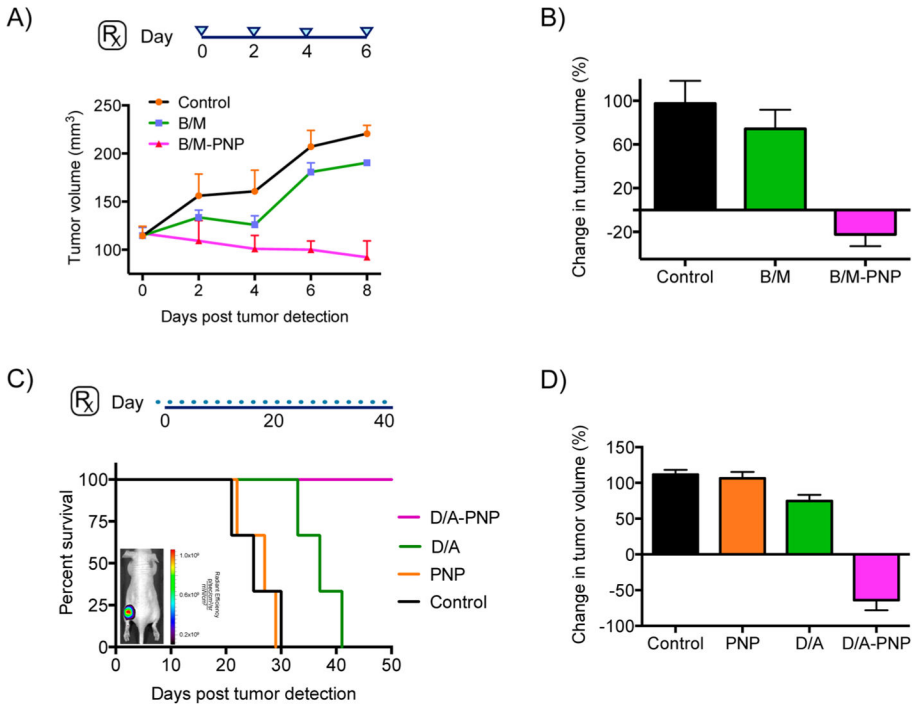

Figure 5.

Improved combinatorial therapy in vivo with coloaded drug PNPs. (A,B) Athymic, nude male mice with human prostate cancer xenografts of the androgen-receptor-positive cell line LNCaP were treated with PNPs carrying both the PI3K inhibitor BEZ235 and the androgen receptor antagonist MDV3100 (enzalutamide, Xtandi) to simultaneously inhibit these pathways' crosstalk. During the course of a week, and four iv administrations (blue triangles), the PNPs achieved tumor regression, as opposed to the free drugs (B/M = BEZ235/MDV3100; *n* per cohort = 3). (C,D) Improved survival and tumor regression after treatment of athymic, nude female mice that had xenografts of the human breast cancer cell line MDA-MB-468 with PNPs coloaded with doxorubicin and the MEK inhibitor AZD6244 (Selumetinib). The animals were treated every other day during the course of 40 days, through iv administration of the agents (D/A = Doxorubicin/AZD6244; *n* per cohort = 3). Fluorescence-based imaging of naïve, untreated animals showed accumulation of drug-free DiR-loaded PNPs at the tumor 24 h post iv administration (inset). Means ± SEM.

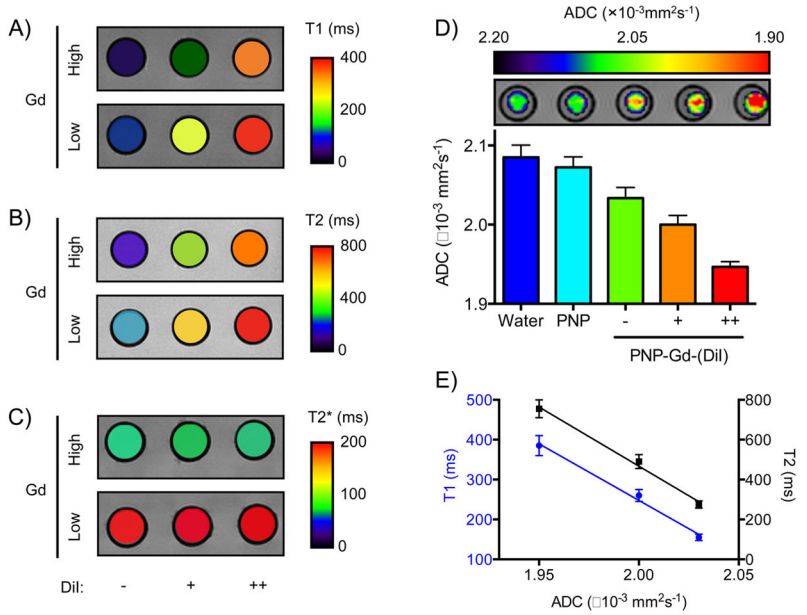

Figure 6.

MRI-based characterization of multifunctional PNP. (A–C) MRI phantom images of Gd-chelating PNP, which were either empty or loaded with cargo (DiI), demonstrating that the cargo affects the T1 and T2 signal, while it leaves the T2* signal unaffected ([Gd], high = 50 nM, low = 20 nM; [DiI], – = 0 nM, + = 5 nM, ++ = 10 nM. Values were averaged over the entire well). (D) Diffusion-weighted MRI identified that the cargo affected the diffusion of water within the PNP (ADC: apparent diffusion coefficient; [Gd] = 50 nM for all wells). (E) The effect on ADC correlated with the changes in T1 and T2 (PNP: empty PNP without both Gd and DiI). Means ± SEM.

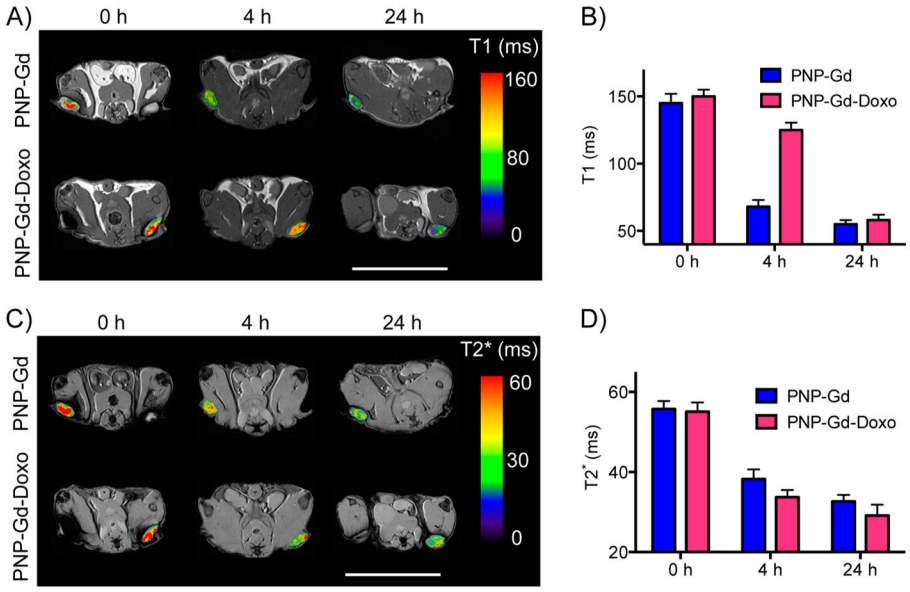

Figure 7.

Imaging of drug-release by the PNP with MRI. (A,B) The release of doxorubicin from PNP coloaded with Gd (PNP-Gd-Doxo) was monitored by measuring the tumor's T1 signal, following accumulation of the PNPs to the tumor through the enhanced permeability and retention effect. (C,D) The PNP homing to the tumor was imaged via the T2* signal, showing that the doxorubicin/Gd coloaded PNP accumulated at the tumor similarly to their gadolinium-carrying only counterparts (PNP-Gd). (scale bars = 25 mm; *n* = 3 per treatment group per time point). Means ± SEM.